Reaction dynamics of metastable helium molecules and atoms near 4.2 K

D. W. Tokaryk, R. L. Brooks, and J. L. Hunt
Guelph-Waterloo Program for Graduate Work in Physics, University of Guelph, Guelph, Ontario, Canada N1G 2W1
(Received 4 January 1993)

Infrared absorption spectra from metastable helium atoms ($2s\ ^3S$, $2s\ ^1S$) and molecules ($a\ ^3\Sigma_u^+$) were previously acquired by irradiating dense helium gas near 4.2 K with a pulsed proton beam [R. L. Brooks, J. L. Hunt, and D. W. Tokaryk, J. Chem. Phys. **91**, 7408 (1989)]. The molecular spectrum was unusual because the observed rovibrational distribution within the $a\ ^3\Sigma_u^+$ state was far from thermal equilibrium. Three different rovibrational groups were observed: (i) $v=0$, $N=1$ ("thermal" molecules); (ii) $v=0$, $9\le N\le 21$ (rotationally excited molecules); and (iii) $10\le v\le 12$, $N=1$ (vibrationally excited molecules). In this work, the time evolutions of members of these three molecular populations were studied both during irradiation and in the subsequent afterglow. In addition, the evolution of the $2s\ ^3S$–$2p\ ^3P$ atomic line was investigated. This study quantitatively explores the reaction dynamics of the metastable molecule in the gas phase near 4.2 K. Gas pressures between 100 and 750 Torr were used. Time-resolved data were taken with a transient-digitizer system and summed for several thousand cycles of the pulsed proton beam. The absorption measurements were converted to time-resolved number densities with the aid of theoretical transition moments. The analysis required that the data be fit to the solutions of sets of coupled differential equations with a nonlinear least-squares-fit routine. The results provide insight into the complicated reactions involved in generating the unusual molecular distribution and into the reactions between the metastable molecules, metastable atoms, and the background helium gas.

PACS number(s): 34.50.Gb, 34.50.Lf, 82.20.Pm

I. INTRODUCTION

Recently, emission and absorption spectra were obtained in dense, cryogenic (near 4.2 K) helium gas subjected to proton-beam irradiation [1,2]. These experiments arose indirectly from the study of infrared absorption features induced in solid hydrogen samples when subjected to the proton beam. During the course of that work, it was found that if a cryogenic hydrogen sample was doped with helium, the proton irradiation induced strong fluorescence from molecular helium (He_2) in addition to fluorescence from helium atoms [1]. The helium seemed to form low-pressure (20–150 Torr) bubbles where dimerization could occur. The features in these spectra attributed to He or He_2 were virtually identical to those taken in pure helium gas near 4.2 K. Several bands of modest intensity were observed in the visible spectrum, but by far the most prominent features were the $d\ ^3\Sigma_u^+ \rightarrow b\ ^3\Pi_g$ and $D\ ^1\Sigma_u^+ \rightarrow B\ ^1\Pi_g$ molecular bands near 6400 Å. Two atomic fluorescence lines, arising from the $2p\ ^3P-3s\ ^3S$ and $2p\ ^1P-3s\ ^1S$ transitions, were reasonably bright as well. Interestingly, while the bright molecular bands showed little vibrational development, a high degree of rotational excitation was observed; the upper-state populations were not in thermal equilibrium with their environment.

In a subsequent experiment, infrared absorptions from the metastable $a\ ^3\Sigma_u^+$ electronic state of He_2 and the metastable $2s\ ^3S$ and $2s\ ^1S$ atoms were observed under proton irradiation in the dense, cold gas. By modulating the proton beam rather than the source lamp, it was possible to detect absorptions as small as 1 part in 10^5 of the full lamp intensity. At pressures near 760 Torr, strong molecular absorptions were detected, but no atomic absorptions could be observed. As the gas pressure was reduced, atomic absorptions became more prominent and molecular absorptions became weaker. The molecular absorption spectrum had a very unusual rovibrational distribution. Prominent spectral lines were found to be due to transitions from the lowest rotational state ($N=1$) of the highest fully bound vibrational levels ($v=12$ to 10) of the $a\ ^3\Sigma_u^+$ electronic state. Additionally, spectral features attributed to the lowest vibrational level ($v=0$) of the $a\ ^3\Sigma_u^+$ state were observed, along with much weaker absorptions originating on the ($v=1$) level. Within these two vibrational manifolds, however, the rotational population was composed of molecules in rotational thermal equilibrium with their environment (represented by only the $N=1$ level at these temperatures) and molecules in highly excited rotational states ($N=9$ to 21). This rotational distribution was first observed by Callear and Hedges [3,4] in dense helium plasmas both at room temperature and at 77 K; in their experiments the distribution quickly thermalized at room temperature, but at 77 K its persistence led the authors to speculate that the molecule was "rotationally metastable" at low temperatures.

The spectra described above were surprisingly similar to those taken in electron-irradiated samples of liquid helium many years earlier [5,6]. This work in the liquid was undertaken to determine the nature of "neutral excitations" found therein [7]. The source of these excita-

tions was found to be excited He_2 and helium atoms [5]; the longer-lived excitations were found to be the metastable species [6]. As in the solid-hydrogen work, the excitations were thought to form as bubbles in the surrounding medium. Interestingly, the observed rotational distributions in the ($v=0$) manifold were identical to those observed in the proton-irradiated cryogenic gas in both the absorption and the emission spectra. Further, absorptions due to the highly vibrationally excited metastable molecules were observed, although their identification as such was not confirmed until the gas-phase experiment was performed several years later.

The observation of excited He_2 far from thermal equilibrium suggests that the reaction kinetics of cryogenic helium plasmas are rather complex. In particular, the molecular absorption spectra seemed to indicate that three different reaction mechanisms were responsible for population of the $a\,^3\Sigma_u^+$ state, one for each of the thermal, rotationally excited, and vibrationally excited components. This paper presents the results of an investigation of the kinetic behavior of the metastable He_2 molecules observed in a cryogenic gas-phase helium plasma. Time-resolved measurements were made of the absorption from metastable He_2 and atomic helium at pressures between 100 and 760 Torr, where the metastable molecule was the dominant excited species. A similar experiment was performed by Keto *et al.* on the absorptions and emissions observed in electron-irradiated liquid helium [8–10]. The present work, however, marks the first time that the gas-phase kinetics of a helium plasma have been investigated at temperatures near 4.2 K. Further, since the spectra taken in the liquid environment had limited resolution, individual rotational levels within the ($v=0$) manifolds could not be timed. Rotational lines were well resolved in the present gas-phase spectra, and have been timed individually. Finally, since the absorptions due to highly vibrationally excited He_2 have now been confidently assigned, the kinetic investigation can fully incorporate measurements on these molecules in an overall description of the behavior of $a\,^3\Sigma_u^+$-state He_2 in a cryogenic helium plasma.

The paper is presented in seven sections. Section II will discuss previous work on the kinetic behavior of metastable helium species in helium plasmas, emphasizing the work on metastable He_2. Section III will present the experimental procedures followed in this work. A discussion of the method used to convert spectral data into number densities of metastable species is given in Sec. IV. A presentation of the data, and of the analysis, follows in Secs. V and VI. Concluding remarks are given in Sec. VII.

II. PREVIOUS WORK ON THE KINETICS OF HELIUM PLASMAS

A. The formation of metastable He_2 in a helium plasma

The majority of previous experiments on the kinetics of metastable species in a helium plasma have been conducted at room temperature and low to moderate pressures of helium gas. Under such conditions, the metastable atomic state $2s\,^3S$ tends to be the dominant metastable species, and its kinetic behavior is well understood. In 1955, Phelps [11] showed that the $2s\,^3S$ state was responsible for the creation of metastable He_2 through the following reaction:

$$^3S+2\mathrm{He}\rightarrow a\,^3\Sigma_u^+ + \mathrm{He}\ . \tag{2.1}$$

This reaction has been invoked in a large number of papers as a source term for the $a\,^3\Sigma_u^+$ metastable molecule, but some subsequent work has shown that the observed reaction rates are too small to account for all of the metastable molecules formed under certain experimental conditions [12,13]. Because the $a\,^3\Sigma_u^+$-state potential curve exhibits a repulsive hump between the attractive well and the $1s2s\,^3S-1s^2\,^1S$ separated-atom asymptote, the rate associated with this reaction has a strong temperature dependence. Measurements of this rate at various temperatures were made by Phelps and Molnar [14] and by Ludlum, Larson, and Caffrey [15]. In the most recent study [16], measurements were taken between 65 and 700 K. Below 65 K, reaction (2.1) could not be detected [17], making this process an unlikely source of metastable He_2 in plasmas near 4.2 K.

Diatomic helium in the $a\,^3\Sigma_u^+$ state can also be formed from the neutralization of ionic species. The most obvious ionic precursor to neutral He_2 is the molecular ion He_2^+. Many processes have been proposed to effect the conversion of He^+ or He* (helium atoms in excited states) to He_2^+:

$$\mathrm{He}^+ + 2\mathrm{He}\rightarrow \mathrm{He}_2^+ + \mathrm{He}\ , \tag{2.2}$$

$$\mathrm{He}^+ + 3\mathrm{He}\rightarrow \mathrm{He}_2^+ + 2\mathrm{He}\ , \tag{2.3}$$

$$\mathrm{He}^*(n\geq 3)+\mathrm{He}\rightarrow \mathrm{He}_2^+ + e^-\ . \tag{2.4}$$

The first process listed is a simple three-body conversion of the atomic ion to the diatomic molecular ion. Several authors have postulated that the resulting ion will be in highly vibrationally excited states. The second process, a four-body conversion mechanism, is included as it has been recently found to augment significantly the first process [18]. Surprisingly, the four-body reaction seems to be significant even at relatively modest helium pressures. The last process, called the Hornbeck-Molnar process [19], can occur because the potential curve for the ground state of the He_2^+ ion is deeply bound; in fact, its minimum of energy lies at the same level as the manifold of helium atomic levels with principal quantum number $n=3$. Helium atoms excited to states with $n\geq 3$ can, upon collision with a ground-state atom, convert directly into the molecular ion and eject an electron. Theoretical work initiated by Mulliken [20] has indicated that the resulting ion is left in a vibrationally excited state, not in the ground vibrational state.

Several authors have investigated the recombination of He_2^+ ions with electrons. Three major mechanisms have been proposed:

$$\mathrm{He}_2^+ + e^-\rightarrow \mathrm{He}^* + \mathrm{He}\ , \tag{2.5}$$

$$\mathrm{He}_2^+ + 2e^-\rightarrow \mathrm{He}_2^* + e^-\ , \tag{2.6}$$

$$\mathrm{He}_2^+ + e^- + \mathrm{He}\rightarrow(\mathrm{products})\ . \tag{2.7}$$

The first of these is a dissociative recombination of the ion into an excited atom and a ground-state atom, the reverse of the Hornbeck-Molnar process. Because of the constraints imposed by Mulliken, the ion must be in a vibrationally excited state to participate in dissociative recombination. Reaction (2.6), commonly called collisional-radiative recombination, involves a collision between two electrons in the vicinity of a He_2^+ ion which slows one electron sufficiently for its capture into high Rydberg states of the He_2 molecule, followed by rapid radiative decay to lower levels [21]. Reaction (2.7) describes the same process whereby a neutral helium atom is used to stabilize this recombination [22]. Rates for the above reactions can be dependent on the temperature of the electrons, which often changes with time during the afterglow.

In 1968, strong evidence was presented for the existence of the He_3^+ ion in a room-temperature helium afterglow [23]. The reaction presumed responsible for the ion was a standard three-body process:

$$He_2^+ + 2He \rightarrow He_3^+ + He \ . \tag{2.8}$$

It was found that as the sample was cooled, the He_3^+ ion formed more and more readily, until at 76 K the rate of reaction (2.8) was found to exceed that of reaction (2.2). Subsequent work determined that the He_3^+ ion was, in fact, the dominant ion in helium afterglows near 76 K [24,25]. The structure of ionic helium clusters has attracted some theoretical interest in recent years [26–28]. Most of the work has focused on the binding energy and ground-state geometric configuration of these species. The basic unit of these clusters has been found to be the He_3^+ ion, to which other helium atoms attach as weakly bound satellites. In its ground state, the He_3^+ ion assumes a linear geometry in which the nuclei are equidistant, separated by about 1.24 Å, compared to the equilibrium separation of about 1.085 Å for the He_2^+. The excess charge is shared among the three nuclei.

Evidence was presented in 1970 that electron-ion recombination processes in a room-temperature plasma might involve the He_3^+ ion rather than the He_2^+ ion, even though the latter species was more abundant [29]. The authors speculated that this process was responsible for a pressure dependence in previously measured ion-electron recombination rates in the plasma, rather than reaction (2.7). Subsequent work by the same authors on the electronic recombination of He_3^+ at 80 K led to the conclusion that the neutralization process probably resulted in an excited He_2 molecule and a ground-state helium atom [30]. Work on the decay of the electron density in a 4.2-K helium plasma showed that the rate of recombination of the electrons with the dominant ion, presumably He_3^+, was rapid and that electrons were continuously regenerated in the afterglow as a result of ionizing collisions between neutral metastable species [31].

The He_4^+ ion has also been observed in both room-temperature and 76-K plasmas [25,29]. Less is known about the formation mechanisms for this ion than for He_3^+. The ratio of $[He_4^+]/[He_3^+]$ was found to be less than unity at all temperatures and to decrease as the temperature was lowered from 300 to 76 K, possibly indicating an energy barrier to its formation. This ion cluster was observed to decay rapidly in the afterglow, possibly as a result of rapid recombination.

Recently Bates has considered a process somewhat similar to dissociation of an excited He_3 complex to explain the formation of excited atoms from helium molecular ions [32,33]. Bates calls this process Rydberg dissociative recombination. While excited atoms have been commonly thought to form from collisional-radiative capture of electrons by He^+ ions in a helium plasma, Collins and Hurt in 1969 found that the time-resolved fluorescence of the $2s\ ^3S-2p\ ^3P$ transition correlated with fluorescence from molecular bands rather than with other atomic fluorescence [34]. They speculated that dissociative recombination of He_2^+ could feed the $2p\ ^3P$ level. Bates has proposed instead that collisions between ground-state helium and excited He_2 molecules with principal quantum numbers greater than 3 can create a He_3 molecule. One of the several decay paths of this molecule could result in a helium atom with a principal quantum number of 2. Emmert *et al.* [35] have successfully incorporated this mechanism in their experiments. A definitive spectrum of He_3 has not yet been reported, although a recent paper attributes some fluorescence observed in dense (1–5 atm) helium plasmas to it [36].

Researchers have proposed several contrasting models to explain the unusual rovibrational distribution of He_2 molecules, in the $a\ ^3\Sigma_u^+$ state, formed in cold helium plasmas. In the liquid-helium experiments of Keto *et al.* [8–10], a delay in the formation of highly vibrationally excited molecules during electron-beam irradiation led the researchers to postulate that these species were formed in some way from the ^3S metastable atoms, while the vibrationally cooler species were formed from neutralization of He_2^+ or associative recombination of excited helium atoms. Callear and Hedges [4] believed that rotationally excited and thermal metastable molecules formed from He_2^* in highly excited Rydberg states quenched collisionally or radiatively. While Callear and Hedges thought that metastable-molecule production ceased very early in the afterglow, a later intracavity laser absorption experiment by Stahlberg *et al.* [37] led to the conclusion that both a flux equilibrium established between destruction and production processes, and rotational relaxation occurred simultaneously to give the observed distribution.

Lawler *et al.* [12] have observed that He_2 in the $a\ ^3\Sigma_u^+$ and $b\ ^3\Pi_g$ electronic states will form vibrationally relaxed ($v=0$) within 20 ns of the termination of the discharge stimulating their afterglow. They observed that if these molecules were to arise from vibrationally cold He_2^+ ions, then the vibrational relaxation of the ion must be extremely rapid since reaction (2.2) is expected to produce a vibrationally excited ion. Some other experimental evidence [38] suggests, however, that the relaxation of the molecular ion is not inordinately rapid.

B. Rovibrational relaxation of the metastable He_2 molecules

Collision-induced transfer of population from higher to lower rovibrational levels has been observed in the He_2

molecule. Some quantitative work has been done on the rotational relaxation of the $e\,^3\Pi_g$ electronic state in a room-temperature plasma at gas pressures between 10 and 36 Torr [39–41], where rotational relaxation was rapid enough to compete with radiative and collisional electronic quenching. Rapid rotational relaxation of the $a\,^3\Sigma_u^+$ metastable molecule has been commonly observed in low- to moderate-pressure discharges at room temperature; for example, this process was observed to thermalize the rotationally hot component of the $a\,^3\Sigma_u^+$ ($v=0$) manifold at room temperature in the experiments of Callear and Hedges [4]. Stahlberg *et al.* [37] described the rotational relaxation in their 300-K plasma with a Polanyi-Woodhall exponential-gap-relaxation model [42], but only to the level of qualitative consistency with their data. The recent work of Emmert *et al.* [35], performed in electron-irradiated samples of dense (0.5 to 8 bar) helium gas at room temperature, has successfully employed the Polanyi-Woodhall model in a quantitative manner to describe the rotational relaxation of the $a\,^3\Sigma_u^+$ state. As previously mentioned, the rate of rotational relaxation slows to a remarkable degree as the gas is cooled from room temperature to 77 K [4]. No measurement of this rate has been reported at 4.2 K, although extrapolation of Callear and Hedges's results would lead to the conclusion that the relaxation by this process would be very slow.

Vibrational relaxation has also been investigated in metastable He_2, but only among the first four [($v=0$) to ($v=3$)] manifolds. Callear and Hedges observed that the ratio of populations in the ($v=1$) and ($v=0$) levels decreased exponentially with time. At 77 K, this relaxation was also slowed to the point where it was not detectable. Measurements of room-temperature vibrational relaxation rates have been made by Emmert *et al.* [35], and in very-high-pressure discharges by Takao *et al.* [43], but no further measurements have been made at lower temperatures.

C. Removal of metastable species from a helium plasma

Far more work has been done to describe the removal of metastable species from a helium afterglow than to describe their formation. The work has been ongoing for almost 60 years, and the principal processes responsible for metastable decay now seem clearly defined. They can be partitioned into four distinct groups, which we will state here and subsequently discuss.

(a) Diffusive removal: Destruction of the species upon diffusion to the walls of the reaction vessel.

(b) Collisions with background helium atoms: This is a first-order process, involving only one metastable species in the reaction. Only the ^3S metastable atom seems to be destroyed in this manner, through the metastable-molecule formation process (2.1); no evidence has yet suggested that metastable He_2 molecules are destroyed through collisions with background helium atoms.

(c) Collisions between metastables species: Reactions (2.9) and (2.11) are second-order processes, involving two metastable members of the same species:

$$^3S + {}^3S \rightarrow \text{ion products} , \tag{2.9}$$

$$^3S + a\,^3\Sigma_u^+ \rightarrow \text{ion products} , \tag{2.10}$$

$$a\,^3\Sigma_u^+ + a\,^3\Sigma_u^+ \rightarrow \text{ion products} . \tag{2.11}$$

(d) Collisions between metastable species and electrons (often referred to as "superelastic" collisions):

$$^3S + e^- \rightarrow \text{He} + e^- , \tag{2.12}$$

$$a\,^3\Sigma_u^+ + e^- \rightarrow 2\text{He} + e^- , \tag{2.13}$$

$$^1S + e^- \rightarrow {}^3S + e^- , \tag{2.14}$$

$$^1S + e^- \rightarrow \text{He} + e^- . \tag{2.15}$$

Early experiments on the decay of metastable species in rare-gas afterglows were performed by Meissner and Graffunder [44] and by Ebbinghaus [45]. In the early 1950's, Biondi observed that the electron density in his helium plasmas increased after termination of a stimulating discharge [46]; he concluded that collisions between metastable atoms led to significant ionization in the sample [47] in accordance with reactions in group (c) above. Phelps and Molnar [14] subsequently made a measurement of the rate of reaction (2.9), and discovered that the ^3S metastable atom was destroyed in ternary collisions with the background gas; as mentioned in Sec. II A, Phelps [11] later identified the $a\,^3\Sigma_u^+$-state metastable molecule as a product of this reaction. Phelps's experiments also made quantitative measurements of reactions (2.12) and (2.14). Since that time, the veracity of the listed reactions involving the ^3S metastable atom has been established through a large number of experiments conducted to measure the reaction rates; some papers not discussed in this text are given in Refs. [48–51]. Little of the work has involved the ^1S metastable atom; the concentration of this species was often very low compared to that of the ^3S, and its removal from the afterglow significantly more rapid, so it was ignored in many analyses. In most of the experiments involving the ^3S metastable, the experimental conditions (typically, low-density room-temperature plasmas) allow for significant losses of it through diffusion, and the diffusion rate has been frequently measured in conjunction with the rates of various reactions.

In a few instances, the rates of the ^3S reactions have been determined as functions of temperature. The temperature dependence of reaction (2.1) has been discussed in Sec. II A. Ludlum, Larson, and Caffrey [15], determined the rate of reaction (2.9) at 77 K, and Fugol, Grigoraschenko, and Myshkis [52], made determinations of this rate at 300, 120, 80, and 10 K. Compared to the rate of reaction (2.1), the rate of reactive collision between ^3S atoms is only moderately temperature dependent; Fugol's measurement at 300 K was only about twice that determined at 10 K. Determinations of the rate of ^3S diffusion [53] have been made as a function of temperature to 4.2 K. Because of the repulsive barrier in the $a\,^3\Sigma_u^+$-state potential curve, the diffusion rate decreases steadily with temperature.

Less work has been done on the kinetic behavior of metastable molecular helium than on the behavior of the ^3S atom. When Phelps noted the presence of $a\,^3\Sigma_u^+$-

removal processes other than diffusion in his work [11], he speculated that collisions with low-energy electrons or with other metastables (of any sort) could be the cause. His speculations were confirmed by Ludlum, Caffrey, and Larson [49] who observed the effects of electron collisions on the molecular metastable density, and by Callear and Hedges [4], who found that the overall decay of the He_2 $a\ ^3\Sigma_u^+$-state population was second order in the absence of other metastable reactants, in accordance with reaction (2.11). In neither experiment were the rates of the reactions determined, however.

The first measurements of k_{MM}, the rate of reaction (2.11), were made in the liquid-helium experiments referred to in Sec. I, first by Hill, Heybey, and Walters [6] and subsequently by Keto *et al.* [9]. In this environment, the decay of molecular metastable species was well modeled by a second-order decay function. Subsequent measurements were made in low-pressure room-temperature gas discharges, as part of three experiments in which many of the loss processes discussed above, as well as several of the ion reactions and recombination mechanisms discussed in Sec. II A, were simultaneously considered in the analysis [54–56]. In these experiments, time-resolved density measurements of the atomic and molecular helium metastable species, and of the electrons, He^+ ions, and He_2^+ ions in the sample, were fit to the solutions of coupled differential equations in which the reaction rates and diffusion coefficients were variable parameters. This procedure permitted the determination of the rate k_{MT} of reaction (2.10) (T denotes the triplet metastable atom $2s\ ^3S$) and the rate k_{Me} of reaction (2.13), as well as k_{MM} and the rates of processes involving the atomic ^3S metastable. Because of the complex coupling of the molecular metastable decay to that of other species, the decay curves followed no particular kinetic order. The most recent determination of the rate k_{MM} was made in a room-temperature plasma at high pressure (760 to 3000 Torr), in which the loss of $a\ ^3\Sigma_u^+$-state He_2 to diffusion or collision with electrons was not important [57]. Under these conditions, the helium molecular metastable decay could be described only by mutual collisions [reaction (2.11)] and by collisions with a trace amount of neon present as an impurity.

The last point underscores the importance of gas purity in obtaining consistent results in work of this nature. Because of the Penning ionization process, trace amounts of an impurity will efficiently remove metastables from the afterglow. Since the metastable concentrations are usually small compared to the concentration of the ambient helium gas, even ppm concentrations of impurity will equal or exceed that of the metastables. Under cryogenic conditions, impurities will freeze to the walls of the experimental vessel and will not react with the metastable species.

Previously determined values for the molecular reaction rates k_{MT}, k_{MM}, and k_{Me} are given in Table I. There is little consistency between the various determinations of each constant, partly due to a lack of information about the molecular transition moments used to convert absorption profiles into absolute number densities of metastable molecules. Most researchers have relied on sensible estimates of the transition moment or have employed consistencies in their fitting data to eliminate the transition probabilities. A measurement of the lifetime of the $e\ ^3\Pi_g$ electronic state [41] permitted determination of the transition probability linking this state to the $a\ ^3\Sigma_u^+$ state, but it was made subsequent to most of the experiments discussed above. Recently, however, a set of *ab initio* calculations by Yarkony [58] has included transition moments linking the $a\ ^3\Sigma_u^+$ state to both the $b\ ^3\Pi_g$ and $c\ ^3\Sigma_g^+$ states; this calculation will be used in the present work.

III. EXPERIMENT

A. Procedure

Experiments were performed at both the Tandem Accelerator Laboratory in McMaster University, and the University of Guelph. In both facilities the apparatus was arranged on an optical table at the end of the accelerator beam line. The schematic diagram given in Fig. 1 represents the arrangement employed in the McMaster experiments; the grouping of equipment was slightly different in the Guelph experiments, but was functionally identical. Only those components new to the timing measurements will be discussed here; otherwise, see Ref. [2].

Proton-beam energies between 8 and 10 MeV were employed in the experiments at McMaster, where the nickel foil, through which the proton beam passed into the sample, was 125 μm thick; this resulted in a post-foil beam energy between 3.2 and 6.4 MeV. At Guelph, the accelerator was run at 3 MeV through a 10-μm-thick foil, resulting in a 2.4-MeV beam incident on the sample. Typically, the modulated beam current was maintained at 10 nA as collected in a Faraday cup through averaging electronics. Since the duty cycle for the modulation was

TABLE I. Previously determined rates for reactions involving molecules in the metastable $a\ ^3\Sigma_u^+$ state of He_2. The designation T_e refers to the electron temperature (in K).

k_{MM} (10^9 cm^3/s)	k_{MT} (10^9 cm^3/s)	k_{Me} (10^9 cm^3/s)	Temperature (K)	Pressure (Torr)	Reference
0.3			2	Liquid	6
0.1 to 0.7			2 to 1.4	Liquid	9
3.85±0.5	0.40±0.04	1.7±0.4	300	1.86	54
0.5±0.2	2.5±1	$(0.09\pm0.02)\sqrt{T_e}$	300	7 and 40	55
1.5±0.5	2.5±1.5	3.8±0.8	300	5–100	56
0.13±0.03			300	1000–3000	57

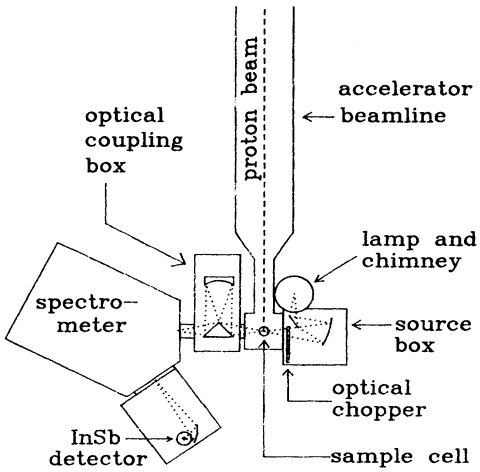

FIG. 1. Schematic diagram of the experimental layout at McMaster. The paths of the light rays (excluding those through the spectrometer) are shown as dotted lines.

always 50% or less, the current available during the "on" cycle ranged from 20 to 40 nA.

The experiment involved recording both an infrared absorption spectrum and timing curves for several of the observed features. Briefly summarized, when the source lamp was left unmodulated but the proton beam was chopped, the concentration of metastable species was observed to modulate at the beam-chopping rate. Thus, at frequencies where the metastable species absorb, a small fraction of the lamp signal would modulate at the beam rate, and could be discriminated from the high dc background with the lock-in amplifier. Initial inspection of the timing curves showed that the chopping rate of 330 Hz used in Ref. [2] was too rapid to establish steady-state conditions in either the turn-on or turn-off portion of the duty cycle; this frequency was reduced to appropriate values between 10 and 40 Hz. A duty cycle of 50% was used for all spectral data collection. The signal was maximized at slightly different phases for each spectral line, but the greatest difference between two lines was only 15°, so spectra were collected at a phase halfway between the extremes. A cooled InSb detector was employed in this experiment, which had a considerably faster response time compared to the PbS detector used in our previous work.

Although a background spectrum of the source lamp through an empty cell was not necessary to detect spectral lines, one was required to assess the absorbance in each line. Background spectra were recorded with the proton beam off; the lamp itself was modulated with a fan chopper.

Timing curves were acquired with a DSP Model 2030 8-bit transient digitizer, to collect a time-resolved absorption pattern during one cycle of the proton beam, and a DSP Model 4001 signal-averaging memory unit, which summed patterns acquired over several thousand cycles, thereby averaging statistical noise out of the data. In this mode, the lock-in amplifier was used only as an ac amplifier of variable gain, the output of which was presented to the transient digitizer. During the course of one proton-beam cycle, data were collected by the transient digitizer at regular intervals ranging from 3.3 to 20 μs. Between 5000 and 25 000 digitized curves were summed during the collection of a single time-resolved pattern.

B. Temperature

We have carefully considered both the temperature of our sample cell and that of the gas. We have calibrated our cell temperature by monitoring the vapor pressure of hydrogen gas above a liquid- or solid-hydrogen sample (12–20 K) and above a liquid-helium sample (3.5–4.2 K). Temperatures below 4.2 K can be achieved by pumping on the exhaust of the cryostat. We determined that, above 12 K, the temperature of the cell was within 0.3 K of the temperature given by the thermometer on the cold-finger itself. At 3.6 K, the cold-finger temperature read 2.5 K, indicating a maximum error of 1.1 K.

The temperature of the gas when the proton beam is on the sample is another matter. With liquid helium in the cell, and the beam on, the vapor pressure indicated a temperature rise for only 0.3 K compared to the beam-off temperature. Hence, the beam does not warm the cell unduly. To estimate the gas temperature, we used the standard heat-transport equation, assumed uniform heating of the sample, made a spherical approximation (0.5 cm radius) for the sample, and took the thermal conductivity of helium gas to be [59]

$$\left[0.17\ \mathrm{mW\,cm^{-1}\,K^{-1}}\right]\left[\frac{[T\ (\mathrm{K})]}{10\ \mathrm{K}}\right]^{1/2}. \tag{3.1}$$

For the worst case, 2.4 MeV of the beam energy was delivered to the sample gas at 750 Torr pressure. Using 10 nA of current, a cell-wall temperature of 5.5 K, and 100% gas heating efficiency, one obtains a temperature of 16.4 K at the center of the cell. For a more typical case, 1 MeV was delivered to the gas, and using 50% efficiency and 350 Torr pressure, the central temperature would be 7.0 K.

The rotational distribution of the cold molecules itself offers a direct, though imprecise, measure of the gas temperature. Based on our sensitivity, this method of temperature determination yields <20 K. Throughout this paper we will refer to temperature as that measured by our thermometer on the cold finger. No strong temperature or density effects of the background gas are expected under these conditions, and the relevant metastable concentrations have been measured spectroscopically. Additionally, the thermal relaxation time is long (~ 7 s) compared to the chopping time, so little perturbation of the timing curves will occur due to thermal transients.

IV. CONVERSION OF SPECTRAL DATA TO METASTABLE-SPECIES NUMBER DENSITY

A. Determination of oscillator strengths for the $b\ ^3\Pi_g \leftarrow a\ ^3\Sigma_u^+$ spectral features in He_2

Oscillator strengths for transitions in atomic helium can be found in Wiese [60]; the $2s\ ^3S-2p\ ^3P$ oscillator

strength is given as 0.5391. No measurements of the transition probabilities of rovibrational lines in the $b\,^3\Pi_g \leftarrow a\,^3\Sigma_u^+$ electronic transition of He_2 were known to us, so the *ab initio* calculation by Yarkony [58] of $\mu_\perp$, the electronic transition moment connecting these states, has been used in this work to evaluate the oscillator strengths for the observed absorption lines.

The expression for the line intensity S_{12} for a transition between a particular rotational level 1 (as defined by Whiting *et al.* [61]) in the lower electronic state and a rotational level 2 in the upper state can be written

$$S_{12} = |\langle v' | R_e(r_i) | v'' \rangle|^2 \beta_{12} , \tag{4.1}$$

when factored under the Born-Oppenheimer approximation [61,62]. The term β_{12} is the rotational line strength factor, and the other term describes the combined effects of the electronic and vibrational wave functions on the line intensity. The quantity $R_e(r_i)$ represents the matrix element of $\mu_\perp$ between the electronic wave functions, parametrized by the internuclear distance r_i; this is the quantity evaluated by Yarkony. v' and v'' are the vibrational wave functions for the upper and lower states. Vibrational wave functions were obtained by using the $a\,^3\Sigma_u^+$- and $b\,^3\Pi_g$-state potential curves (as calculated by Yarkony) as input into a program by LeRoy [63]. The program was suitably modified to allow the input of $R_e(r_i)$ as well, and to calculate the vibrational-electronic matrix element $\langle v' | R_e(r_i) | v'' \rangle$. Because of the interaction between the vibrational and rotational motions of the molecule, different vibrational wave functions (and different vibrational-electronic matrix elements) were obtained for every rotational level observed in the spectrum. Between vibrational bands, the differences were more acute due to changes in the Franck-Condon factor; for example, the vibrational-electronic matrix element for $Q(1)$ lines of the (0-0), (10-10), (11-11), and (12-12) bands were 2.6548, 2.5827, 2.4133, and 1.9144 a.u.

The rotational line strength factors β_{12} can be evaluated using the formal procedures of Hougen [64] or Whiting and Nicholls [62]. They are also tabulated in a book by Kovacs [65]; however, the expressions given in the book must be doubled for consistency with the Whiting convention [61]. Once the rotational line strength factors are obtained, the full line strengths S_{12} can be calculated for each rotational line, and converted to oscillator strengths through the relationship given by Schadee [66]:

$$f = \frac{8\pi^2 m_e \nu}{3he^2} \frac{S_{12}}{(2J+1)} . \tag{4.2}$$

In this formula, the quantity ν is the transition frequency in s^{-1}, and the J is the quantum number for the total angular momentum of the lower state; the other constants have their usual meanings. We have assumed that molecules are distributed statistically within a single N multiplet. Effective oscillator strengths for the observed lines can be constructed by weighting the oscillator strength for each line by the fraction of population in the associated lower J level, summing the results, and dividing by the total number of states.

The results of the oscillator strength calculations for the observed $b\,^3\Pi_g \leftarrow a\,^3\Sigma_u^+$ rovibrational lines in He_2 are given in Table II. For the (0-0) vibrational band, the transition frequencies were calculated with the standard spectroscopic formulas using constants given in Rogers *et al.* [67]. For the vibrationally excited transitions, the frequencies are taken directly from Ref. [2].

TABLE II. Effective oscillator strengths for selected rovibrational transitions of the $b\,^3\Pi_g \leftarrow a\,^3\Sigma_u^+$ electronic transition in He_2, evaluated with the theoretical transition moment of Yarkony [58].

		For the (0-0) band			
$R(1)$	0.102 64	$Q(1)$	0.102 07		
$R(3)$	0.073 70	$Q(3)$	0.102 04	$P(3)$	0.029 00
$R(5)$	0.065 98	$Q(5)$	0.101 98	$P(5)$	0.036 65
$R(7)$	0.062 49	$Q(7)$	0.101 89	$P(7)$	0.040 01
$R(9)$	0.060 56	$Q(9)$	0.101 79	$P(9)$	0.041 77
$R(11)$	0.059 35	$Q(11)$	0.101 65	$P(11)$	0.042 84
$R(13)$	0.058 54	$Q(13)$	0.101 50	$P(13)$	0.043 47
$R(15)$	0.057 98	$Q(15)$	0.101 33	$P(15)$	0.043 85
$R(17)$	0.057 56	$Q(17)$	0.101 13	$P(17)$	0.044 05
$R(19)$	0.057 24	$Q(19)$	0.100 92	$P(19)$	0.044 13
$R(21)$	0.056 99	$Q(21)$	0.100 69	$P(21)$	0.044 13
		For the (10-10) band			
$R(1)$	0.102 50	$Q(1)$	0.102 09		
		For the (11-11) band			
$R(1)$	0.093 08	$Q(1)$	0.092 26		
		For the (12-12) band			
$R(1)$	0.061 86	$Q(1)$	0.060 74		

B. Assessment of number density from spectral data

The intensity of a line in the absorption spectra is proportional to the amplitude of the fundamental Fourier component (the component at the frequency of the pulsed beam) of the wave form received from the detector by the lock-in amplifier. Thus, the intensity is proportional to the number density of metastable species at steady state just before the proton beam is terminated. The number density at other points on a timing curve can be assessed by appropriate scaling.

Once the absorption spectra are cast in the form $\ln(I_0/I_\sigma)$ versus σ, the integral over a spectral line can be related to N, the number density of absorbers giving rise to the line, through a simple formula given by Thorne [68], suitably modified for an ordinate in wave numbers:

$$\int_{\text{line}} k_\nu d\nu = c' \int_{\text{line}} k_\sigma d\sigma = \frac{c'}{l} \int_{\text{line}} \ln\left[\frac{I_0}{I_\sigma}\right] d\sigma = \frac{e^2}{4\epsilon_0 m_e c} N f \ . \tag{4.3}$$

Here, k_ν and k_σ, each with units m^{-1}, represent the absorption per unit path length as functions of frequency ν (in s^{-1}) and wave number σ (in cm^{-1}). The dimensions of N are m^{-3}, the path length l has dimensions of meters, and the oscillator strength f is dimensionless. The other constants have their usual meanings, and are expressed in SI units, except that c' is the speed of light in cm/s for compatibility with the wave-number units in the associated integral.

Integrals over the spectral features were evaluated by fitting the lines to single Gaussian functions. The path length l is not uniform in this experiment, since the excitation volume of the proton beam defines a cylinder as it passes through the sample. However, since the strongest absorption we detect is about 0.5% of the total lamp intensity, the samples are optically thin. Under these circumstances, we may evaluate an equivalent path length for a sample of constant thickness, based on the geometry of our excitation volume.

Under some experimental conditions, the transitions observed in absorption are also strongly observed in emission. In such a situation, account must be taken of the fluorescence signal in determining the density of absorbers in the sample. Several attempts were made to detect infrared fluorescence of the $b\ ^3\Pi_g \rightarrow a\ ^3\Sigma_u^+$ band using pulsed-beam emission techniques, but no infrared emission signal was observed in the vicinity of the molecular bands, so no correction for emission was made when evaluating the density of molecular metastables.

Our absorption spectrum shows small lines between members of the (0-0) P branch. These lines are rotationally excited lines of the (1-1) vibrational band. The $R(1)$ and $Q(1)$ lines of this band give rise to the intensity anomalies in the $Q(1)$ and $Q(11)$ lines of the (0-0) band. The trace presence of unresolved (1-1) band spectral features in the Q and R branches of the (0-0) band, as well as the general congestion of these bands, made them unsuitable for the determination of numbers densities of rotationally excited (0-0) lines. Only lines in the P branch were used for this purpose.

Uncertainties in the number densities obtained with these methods arise from several sources. Quantitative uncertainties arise primarily from the equivalent path length and from statistical error in the Gaussian fits to the spectral lines. Statistical error was obtained directly from the nonlinear least-squares-fitting program used to obtain the Gaussian parameters. Background noise was assumed to be representative of the statistical fluctuations in the data, and was assessed by averaging the signal level over 50 data points in a flat spectral region and evaluating the standard deviation of data from the average value. This approach seemed justified because the primary source of background uncertainty was detector and lamp noise, rather than signal fluctuations. Unlike photon counting, where the number of counts follows a Poisson distribution, the signal in this experiment was relatively uniform compared to the high level of the background lamp.

Systematic uncertainties could also affect the spectral data, and hence the number densities obtained from them. At the cryogenic conditions of these experiments, residual gases in the target area could freeze to the cell windows, degrading their transmission properties. This effect is cumulative during the time that the sample cell is cold. Also, because the wave forms for each timing curve (and for the chopped background lamp) were different, the percentage of the total wave form attributable to the fundamental Fourier component would vary by a small amount between wave forms; only this component would be detected by the lock-in amplifier. The slight differences in optimal phase for each spectral line mentioned in Sec. III A contribute a systematic error as well.

V. DATA

Time-resolved absorption data were obtained at six different pressures and at various proton-beam energies and currents. Table III lists the experimental conditions under which each data set was taken. The Table also lists the percentage of metastable molecules and atoms in the total steady-state population. The atoms are seen to make up only a vanishingly small percentage of the total number of metastable species in all of the data taken at McMaster (except at 100 Torr), but are present in reasonably high numbers in the two Guelph data sets, where the proton-beam energy was much lower. Typically, at a given pressure, timing curves would be collected for the $R(1)$ and $Q(1)$ lines of the $b\ ^3\Pi_g \leftarrow a\ ^3\Sigma_u^+$ (12-12) band (representing the vibrationally highly excited species), the $P(17)$ line of the (0-0) band (the strongest well-resolved rotationally excited line), at least one other rotationally excited line, the $R(1)$ line of the (0-0) band (representing the thermal population), and, if possible, the $2s\ ^3S - 2p\ ^3P$ and $2s\ ^1S - 2p\ ^1P$ lines.

Figure 2 shows plots of the number density as a function of time for representative lines in each of the three population groups associated with the $a\ ^3\Sigma_u^+$ metastable molecule at 500 Torr. One can see immediately that these three populations have very different timing charac-

TABLE III. Experimental conditions and relative percentages of steady-state metastable populations for the absorption data analyzed in this work.

Pressure (Torr)	Post-foil beam energy (MeV)	Unchopped-beam current (nA)	Metastable molecules (%)	^3S atoms (%)	^1S atoms (%)
		McMaster data			
760	6.3	30	100		
500	3.2	40	99.3	0.7	
300	3.2	40	95.7	2.9	1.4
100	5.4	40	69.4	23.6	7.0
		Guelph data			
400	2.4	25	85.0	11.2	3.7
200	2.4	25	76.0	18.6	5.4

teristics. The vibrationally excited population, represented here by the $R(1)$ (12-12) line, increases rapidly with the proton beam, and decays away faster than the other metastable populations. The rotationally excited population, illustrated here with the $P(17)$ (0-0) line, also rises quickly during the beam-on phase of the proton beam, but decays more slowly than the vibrationally excited species. The behavior of the thermal levels, shown with the $R(1)$ (0-0) line, is very different from that of the more excited levels. Molecules in this level appear not to form from primary beam products, but are produced from a secondary source. Both the turn-on data, in which the thermal level curve starts out with essentially zero slope and grows nonlinearly with time, and the turn-off data, in which a slight "bulge" can be seen in the first few microseconds (indicative of formation of this level even in the absence of the proton beam), lead to this conclusion. The qualitative features of the timing curves for the three metastable molecule populations do not change significantly with pressure, although the time required to reach steady-state concentrations while the beam is on the sample, and the time for the populations to relax to zero in the afterglow, generally increase as the pressure is reduced.

Figure 3 shows a plot of the $N=15$, 17, and 19 beam-

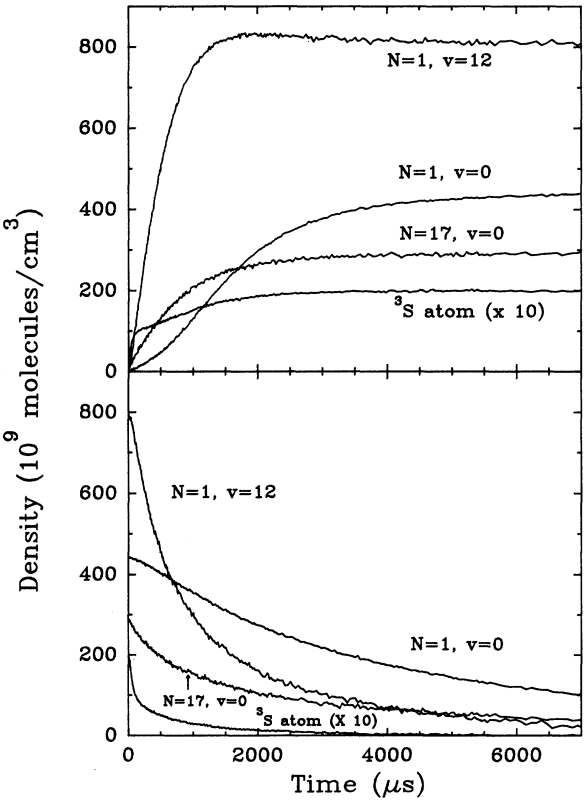

FIG. 2. Turn-on and turn-off timing curves for the $b\,^3\Pi_g \leftarrow a\,^3\Sigma_u^+$ $R(1)$ (12-12), $P(17)$ (0-0), $R(1)$ (0-0) lines in He_2 at 500 Torr, and the $2s\,^3S-2p\,^3P$ atomic He line.

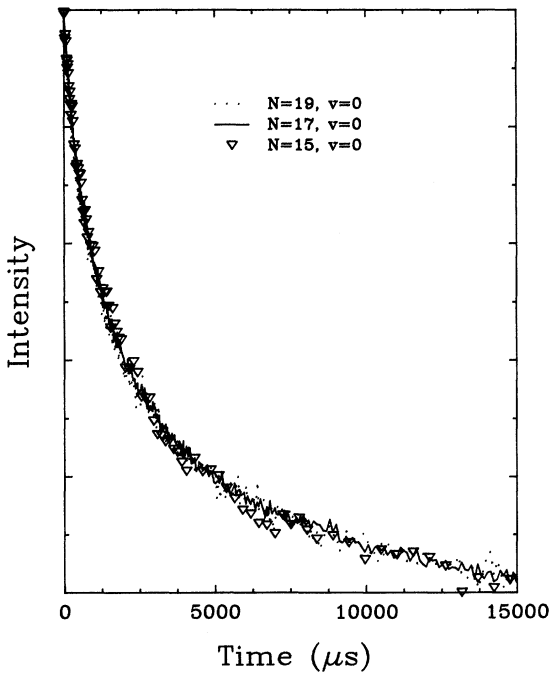

FIG. 3. Decay curves for the $v=0$; $N=19$, 17, and 15 rotational levels of the $a\,^3\Sigma_u^+$ state of He_2 taken at 760 Torr, normalized to a common value.

off timing curves scaled to a common value along the ordinate. The curves appear coincident, which implies that they differ only by a multiplicative constant. Thus, the majority of the rotationally excited population seems to decay by the same process independent of rotational quantum number.

Figure 4 shows the time evolution of the number density of the ^3S atom during the beam-on and beam-off phases at pressures of 500, 300, and 100 Torr. The behavior at high pressures can be characterized by an initially rapid change in concentration, followed by a region of moderate change in the approach to steady state, for both the turn-on and turn-off curves. As the pressure is reduced, the two regions merge into a smoothly varying concentration. The ^1S metastable atom concentration was always observed to be lower than that of the ^3S, and its growing in and decay times were far more rapid than for any other metastable observed in the sample, so this species could be safely ignored in the data analysis.

To ensure that the proton beam was being chopped cleanly, the beam current was read from a Faraday cup located just before the sample, and fed through a 15-kΩ resistor to ground. The voltage drop across this resistor was used as input to the lock-in amplifier, and then into the transient digitizer system. The data show that complete turn-on or turn-off of the current occurs in about 100 μs, and even this time is probably caused by an RC time constant introduced through the Faraday-cup capacitance and the 15-kΩ resistor. The proton-beam response time, in any event, is very short compared to the decay time of most of the metastable species in the sample cell. The InSb detector had a response time quoted by the manufacturer as less than 5 μs and should not be responsible for any structure observed in the decay curves.

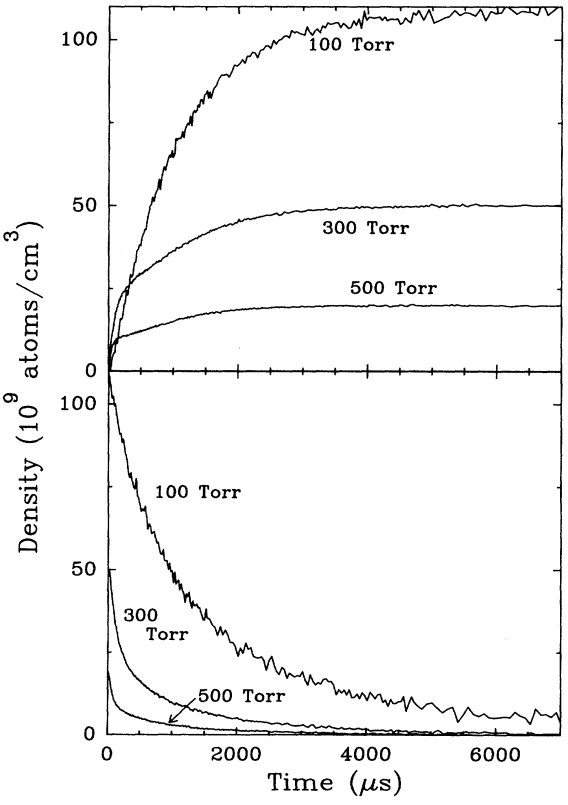

FIG. 4. Turn-on and turn-off timing curves for the ^3S metastable atom at 500, 300, and 100 Torr.

Statistical uncertainty in the absorption timing curves was assumed to be a constant value at all points along the curve, independent of the signal level. This assumption could be justified by evaluating the standard deviation of the data from a straight line in the region of steady state and in the region of zero absorbance. In both regions, this value was the same irrespective of the number density of the absorbers. This uncertainty was combined in quadrature with the uncertainty in the number density assessed from the spectrum when converting a timing curve from arbitrary units to number density versus time.

VI. ANALYSIS

A. The fitting program and procedure

Although timing data were taken during the entire modulation cycle of the proton beam, quantitative analysis was performed only on the afterglow, where the electron and ion densities (which we could not measure) would be much less important than during stimulation. When possible, the data were fit to analytic functions; however, much of the analysis involved fitting the data to models that resulted in a set of coupled differential equations, the solutions of which described the time evolution of each metastable species. The sets of equations were solved numerically with a Runge-Kutta procedure. The fitting program was designed around an algorithm by Marquardt, as employed by Bevington [69]. Uncertainties in the fit parameters were also calculated by the program based on the method described in Bevington.

Each raw timing curve was composed of up to 8192 data points. Logarithmic selection was used to reduce the number for analysis to the range 300 to 500 points.

B. Diffusion and the electron density

Before proceeding with the analysis, some considerations of the effects of diffusion and electron density on the metastable population are in order. Studies of the diffusion coefficient of the ^3S metastable atom have been conducted as a function of temperature [53] to 4.2 K. Because of the repulsive long-range potential between the ^3S metastable and a ground-state helium atom, as a result of the "hump" in the He_2 $a\,^3\Sigma_u^+$-state potential, the diffusion rate decreases dramatically as the ambient gas is cooled, until at 4.2 K its value is only $0.35/p$ cm^2/s, where the pressure p is expressed in Torr. If we assume that the sample cell is uniformly populated with metastables within the cylinder defined by the proton beam (with no population outside this volume) and that the cell interior is cylindrical with a radius R_{cell} equal to that of the nickel foil through which the proton beam is admitted,

then the time constant for the fundamental mode is 7.31 s at 100 Torr. Clearly, this value is extremely long compared to the ~40-ms extent of the longest timing curve measured in these experiments. More of the initial metastable population is in the fundamental mode in the experiments performed at McMaster, where the radius of the excitation volume is equal to R_{cell}, than in the Guelph data, where the excitation radius is about half that of R_{cell}; nonetheless, modes that have time constants comparable to 40 ms are of high order and will have very little effect on the decay in either case. For the ^3S atom, then, we do not expect that diffusive decay will be a significant fraction of the overall decay of the species.

The diffusion coefficient for the $a\ ^3\Sigma_u^+$-state He_2 molecule has been determined only a few times and only at room temperature. This quantity was determined in the experiments of Phelps [11] ($[289\pm47]/p$ cm^2/s), Deloche *et al.* [56] ($[305\pm10]/p$ cm^2/s), and in an experiment by Gusinow and Gerber [70] ($[370\pm35]/p$ cm^2/s); here p is the gas pressure in Torr at 300 K. Without knowledge of the potential between an $a\ ^3\Sigma_u^+$-state molecule and a helium atom, we cannot scale the $a\ ^3\Sigma_u^+$-state diffusion coefficients to 4.2 K; however, we can reasonably infer that this potential will be repulsive, and so the diffusion coefficient should decrease as the temperature is lowered. Three pieces of evidence point toward the required repulsive potential: (a) No convincing absorption or emission spectra from the He_3 molecule have yet been reported, indicating a paucity of stable potential surfaces for this species; (b) no previous studies of the reaction dynamics of $a\ ^3\Sigma_u^+$-state molecules have found any reactive interaction between these molecules and the background gas; and (c) the products of He_3^+ recombination seem to be excited He_2 molecules and a helium atom [30]. We cannot analyze the diffusion of the metastable molecule any further, but it seems reasonable to assume its diffusion coefficient will be comparable to that of the ^3S atom, and thus will be negligible under our experimental conditions.

In the afterglow, electrons are produced as a result of ionizing collisions between metastables, and are removed by recombination. The rate of recombination, k_{recomb}, has been measured in a 4.2-K plasma [31] and was found to lie between 2 and 40×10^{-6} cm^3/s for electron temperatures between 100 and 10 K. When metastable molecules M are the dominant metastable species, the change in electron density n_e is described by the rate equation

$$[\dot{n}_e]=k_{MM}[M]^2-k_{\text{recomb}}[n_e]^2\ . \tag{6.1}$$

The electron density will adjust through recombination until the derivative in the above equation is zero; this situation is "quasi steady state." At this point, the ratio of metastable density to electron density is the square root of the ratio of the mutual molecular collision reaction rate to the electron recombination rate. This ratio indicates that in the afterglow, once quasi steady state has been established, the electron density will be at most 2% or 3% that of the metastable molecules if the recombination rate is only 2×10^{-6} cm^3/s, and the rate k_{MM} of metastable-molecular destruction is taken as the average of the room-temperature gas values, 1.2×10^{-9} cm^3/s. This percentage will decrease if either the recombination rate is raised or if the metastable destruction rate is reduced. The previous work described in Sec. II C indicates that the reaction rate between metastable species and electrons is of the same order as that between metastables species, not several powers of ten larger, so the influence of electrons on the afterglow decay curves should be minimal.

C. The overall metastable-molecule decay

We have argued in Sec. VI B that neither collisions with electrons nor diffusion should play a significant role in the destruction of metastable molecules. Since no previous experiments have established a mechanism by which this species is quenched by background gas, the only established reaction path left to explore is that of reaction (2.11) from Sec. II C, quenching through mutual collision. This is a second-order process and can be described by the differential equation

$$[\dot{M}]=-k_{MM}[M]^2\ , \tag{6.2}$$

which has the solution

$$[M]=\frac{[M_0]}{1+k_{MM}[M_0]t}\ . \tag{6.3}$$

The quantity $[M]$ represents the number density of metastable molecules, and $[M_0]$ represents this density at time $t=0$. Exact second-order decay of the metastable molecule was observed in high-density room-temperature and 77-K plasmas by Callear and Hedges [4] and was a principal component of the decay in the work of Myers and Cunningham [57]. In addition, this timing behavior was observed by Hill, Heybey, and Walters [6] and Keto *et al.* [9] in liquid-helium experiments.

To examine the overall timing behavior of the metastable-molecule population, a timing curve was constructed from the sum of the curves for each populated level of the $a\ ^3\Sigma_u^+$ state. For many sets of timing curves, only one or two of the rotational lines were timed, but since Fig. 3 shows that the data for the rotational levels differ only by a multiplicative constant, the curves that were taken could be safely scaled to the total density of rotationally excited molecules. The small contribution of $(v=1)$ molecules was also factored into the rotationally excited contribution to the sum.

In spite of the qualitative differences between the constituent timing curves from the three metastable populations, the summed data sets were found at each pressure to fit very well to a second-order decay function. A typical fit is given in Fig. 5. The ordinate scale is logarithmic to emphasize the worsening statistics at the lower signal levels. The values of k_{MM} obtained with this procedure are listed in Table IV. The values of this constant are comparable to those of the liquid-helium measurements; they fall between the extremes of measurements made in the room-temperature gas. Uncertainties in the rate constant were determined by summing in quadrature the statistical uncertainty in the fit parameter associated with k_{MM} and the uncertainty in $[M_0]$. It is important to note

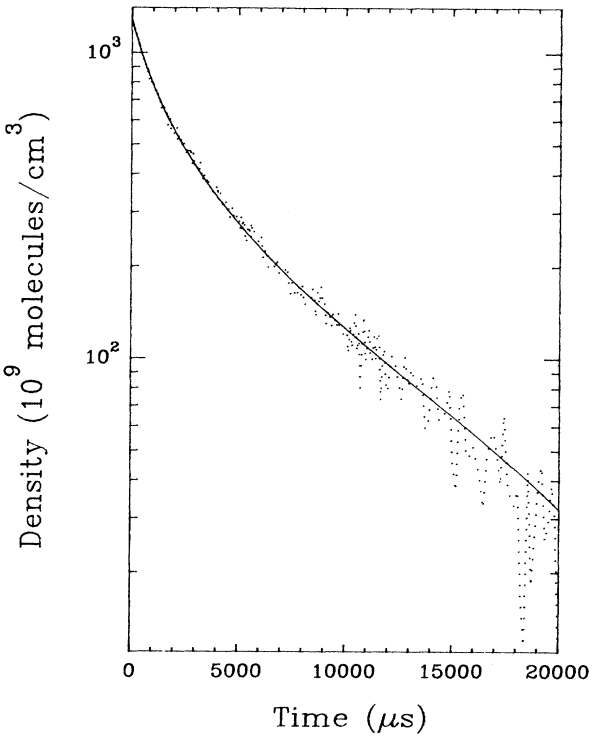

FIG. 5. Semilogarithmic plot of the sum of metastable-molecule concentrations at 300 Torr fit to a second-order decay function.

that while this model is successful, it does not provide any insight into the differences between the timing curves of the three observed metastable-molecule population.

D. Detailed analysis of the metastable-molecule decay

Although the results of Sec. VI C indicate that collisions between metastable molecules play a significant role in the overall decay of the metastable-molecule population, that process alone cannot resolve the differences between timing behavior of the three metastable populations observed. Several different hypotheses were tested to resolve the problem: (a) The value of the reaction rate k_{MM} was assumed to change depending on the rovibrational state of the molecule; (b) the value of k_{MM} was assumed independent of the molecule's rovibrational level, but more excited molecular species were assumed subject to relaxation (rather than destruction) through collision with the background helium gas; (c) some molecular species were assumed to undergo replenishment in the afterglow from the products of mutual metastable-molecule collision; and (d) any combination of process (a), (b), and (c) could occur simultaneously.

TABLE IV. The overall second-order decay rates for the $a\,^3\Sigma_u^+$-state molecules.

Pressure (Torr)	k_{MM} (10^{10} cm^3/s)
760	2.12±0.06
500	2.90±0.07
400	3.85±0.20
300	3.50±0.14
200	2.92±0.14
100	4.98±0.21

Of these alternatives, only models based on hypothesis (c) provided both an excellent fit to the data and physically realistic values for the fit parameters. Such models were cast in the following form:

$$[\dot{V}_{12}] = -k_{MM}[V_{12}][M] + f_{V12}(k_{MM}[M]^2)\,, \tag{6.4}$$

$$[\dot{N}_{17}] = -k_{MM}[N_{17}][M] + f_{N17}(k_{MM}[M]^2)\,, \tag{6.5}$$

$$[\dot{N}_1] = -k_{MM}[N_1][M] + f_{N1}(k_{MM}[M]^2)\,. \tag{6.6}$$

The model expresses rate equations for the evolution of the vibrationally excited $N=1$, $v=12$ level $[V_{12}]$; the thermal level $N=1$, $v=0$ $[N_1]$; and a representative rotationally excited level $N=17$, $v=0$ $[N_{17}]$. The quantity $[M]$ again represents the total metastable-molecule concentration, obtained by summing the $[V_{12}]$, $[N_1]$, and $[N_{17}]$ concentrations after first scaling the latter to the total density of rotationally excited levels. The parameters f_{V12}, f_{N17}, and f_{N1} represent the likelihood that products of the metastable-metastable collision will reform into the associated level. The collision products are expected to be one electron-He_2^+ ion pair and two ground-state helium atoms, so the sum of all regeneration parameters (including those for rotational levels not explicitly measured) cannot exceed 0.5. The parameter f_{V12} was found to converge to a very small number (less than 0.001), and when it was dropped from the model, the overall reduced χ^2 for the system was found to improve slightly, so the parameter was not used in subsequent modeling. Figures 6 to 8 show the data and the fit curve for each of the $[V_{12}]$, $[N_{17}]$, and $[N_1]$ levels timed at 500 Torr.

The model was found to work equally well for data at all pressures irrespective of the significance of the ^3S atomic metastable concentration, a somewhat surprising result considering that the magnitude of the rate constant k_{MT} describing the rate of ionizing collisions between these species was found in previous work, conducted in room-temperature plasmas, to be comparable to that of k_{MM} (see Table I). A summary of the parameters determined for six pressures of helium gas is given in Table V, and a plot of k_{MM} as a function of pressure is given in Fig. 9. The rate constant k_{MM} appears independent of pressure, consistent with the previously published work, although at lower pressures where the metastable-molecule density is lower, some scatter is evident. All fit parameters fell within the quoted error limits when the concentration estimates for the timed levels were adjusted up and down by their error margins, and when the fit was started at $t=500$ μs, where the concentration of vibrationally excited molecules was reduced to about half of its original value. Considering the statistical uncertainties in the fit parameters, the uncertainties in the number density, and the systematic uncertainties discussed in Sec.

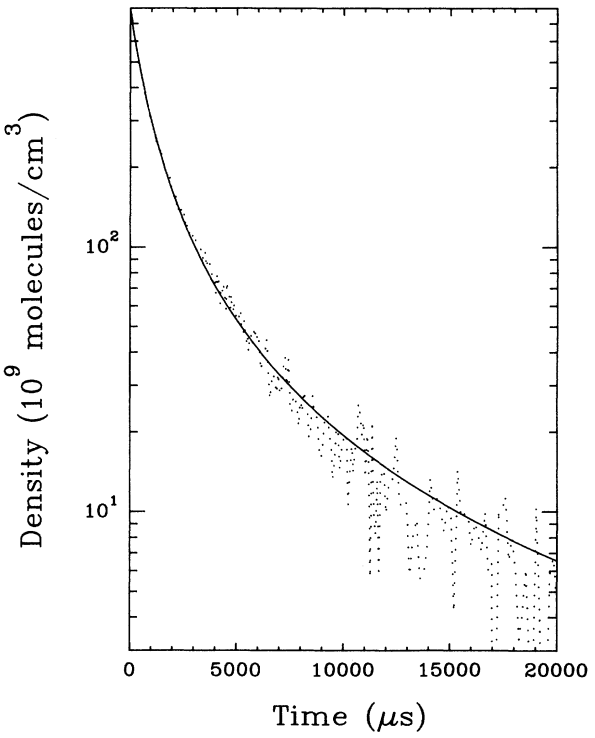

FIG. 6. Semilogarithmic plot of the timing curve for the $N=1$, $v=12$ level at 500 Torr and the fit to the regeneration model.

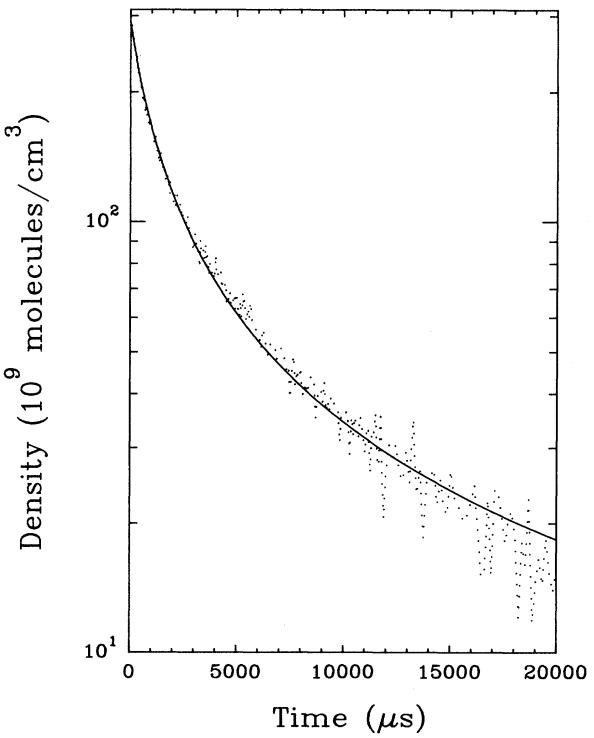

FIG. 7. Semilogarithmic plot of the timing curve for the $N=17$, $v=0$ level at 500 Torr and the fit to the regeneration model.

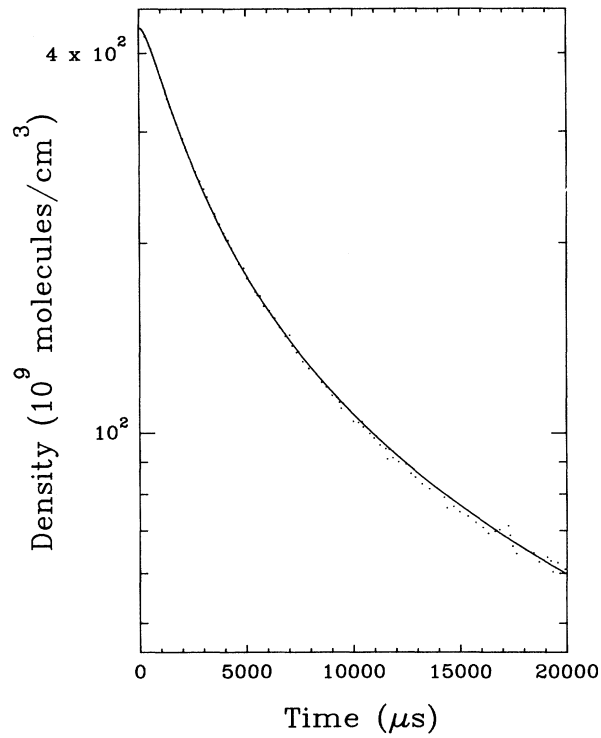

FIG. 8. Semilogarithmic plot of the timing curve for the $N=1$, $v=0$ level at 500 Torr and the fit to the regeneration model.

IV B, we will quote a value of $(5\pm1)\times10^{-10}$ cm^3/s for the rate constant k_{MM}.

E. Analysis of the ^3S metastable-atom decay

Timing curves for the ^3S metastable atom were taken at pressures of 500 Torr and lower. The initially sharp drop in concentration, followed by long-term persistence, is characteristic of the decay curves taken at higher pressure. If we model this behavior with a rapid quenching mechanism, and with regeneration of the metastable atom from the products of metastable-molecule collisions, then we may write

$$[^3\dot{S}]=-k_{\text{quench}}[^3S]+f_{3S}(k_{MM}[M^2]) \ . \tag{6.7}$$

The reaction rate k_{quench} describes some first-order process responsible for rapid quenching, while the parameter f_{3S} is related to the likelihood that the products of an ionizing collision between metastable molecules reforms into a metastable ^3S atom.

This model was found to produce a good fit to the observed decay curves at all pressures; the fit to 500-Torr data is given in Fig. 10. However, the values obtained for k_{quench} and f_{3S}, listed in Table VI, do not give readily interpretable results. The regeneration parameters are unrealistically high, and further, the parameter values (particularly k_{quench}) were not as stable to the initial starting time of the fit as were the metastable-molecule parameter values; we have taken account of this in the uncertainties

TABLE V. Parameters describing the decay of individual rovibrational levels of metastable $a\ ^3\Sigma_u^+$-state He_2 molecules at all pressures considered in this work.

Pressure (Torr)	k_{MM} (10^{10} cm^3/s)	f_{N19}	f_{N17}	f_{N15}	f_{N13}	f_{N1}
760	4.56±0.30	0.033±0.003	0.068±0.004	0.057±0.004		0.226±0.016
500	4.86±0.25		0.045±0.004	0.043±0.003		0.181±0.012
400	5.15±0.45	0.021±0.003	0.027±0.003	0.024±0.003		0.131±0.015
300	5.2±0.4		0.048±0.005	0.029±0.003		0.184±0.015
200	3.8±0.5		0.017±0.002	0.023±0.003		0.135±0.015
100	7.2±1.0	0.053±0.003	0.055±0.006	0.071±0.007	0.043±0.005	0.101±0.012

quoted. The data were reanalyzed with terms involving k_{TT} [the rate for reaction (2.9)], k_{MT}, k_{quench}, and the regeneration ratio f_{3S} in a wide variety of combinations, but in no case was a better fit obtained than in the model originally proposed.

VII. DISCUSSION AND CONCLUSIONS

A. Reactions kinetics of metastable He_2

In these experiments, we were able to address quantitatively the question of the kinetics of metastable He_2. The overall timing behavior, found by fitting the sum of the timing curves for the observed levels of the $a\ ^3\Sigma_u^+$ state to various functions, was found to be second order. Callear and Hedges [4] performed a similar analysis on their data and observed the same qualitative behavior, at temperatures between 300 and 77 K and at several different pressures. Overall second-order behavior was also observed in the experiments performed on electron-irradiated liquid helium, although in that work only the lowest rotational states of the Q branch were timed. In most other experiments, where metastable molecules were not a dominant species, the timing behavior was strongly influenced by interaction with other species, so the second-order decay was not observed.

No rate constants for the overall reaction were evaluated in the work of Callear and Hedges, because the authors did not know the matrix element for the transition they observed. The rate constants quoted in the liquid-helium experiments varied from 2 to 7×10^{-10} cm^3/s, depending on the temperature, but the absolute values were subject to the assumptions made by the authors regarding the matrix element. Rate constants evaluated in our work produced results in the same range as the liquid work for the overall decay, but the results showed a definite scattering with pressure. The scattering, and the qualitative differences observed in the timing curves for the vibrationally excited, rotationally excited, and thermal levels, led to the conclusion that the rate con-

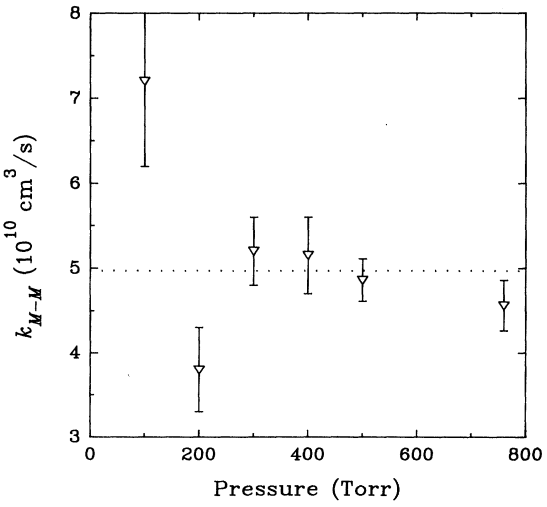

FIG. 9. The rate constant k_{MM} obtained from the six data sets used in these experiments plotted against pressure. The dotted line represents the weighted average of these values.

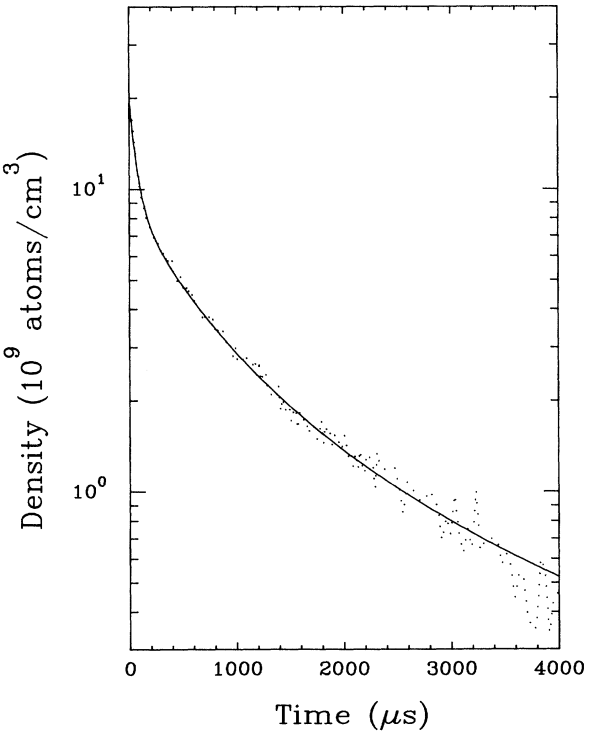

FIG. 10. Semilogarithmic plot of the timing curve for the ^3S metastable atom at 500 Torr and the fit to a model involving first-order quenching and regeneration from collisions between metastable molecules.

TABLE VI. Parameter values for fits of the ^3S metastable-atom timing curves to a model including first-order decay and regeneration from metastable molecule collisions.

Pressure (Torr)	k_{quench} (s^{-1})	f_{3S}
500	15400±1500	0.039±0.005
400	16700±2000	0.420±0.050
300	7600±1000	0.110±0.009
200	5600±600	0.560±0.070
100	1100±250	0.350±0.050

stants determined in this manner were merely effective and did not reflect the true value of the rate constant k_{MM}.

Prior to these experiments, there was some debate in the literature regarding the likelihood of regeneration of the rotationally excited and thermal populations in the afterglow. Callear and Hedges proposed that all of the metastable He_2 was formed in a single batch at the end of their discharge and that reformation of these states in the afterglow was unlikely. Stahlberg *et al.* [37] disagreed with this viewpoint and proposed a scenario in which a flux equilibrium was established between the metastable species and the ion products resulting from their destruction. Analysis of the beam-off timing curves in this experiment clearly favor the conclusions of Stahlberg *et al.* for a 4.2-K high-density plasma. The molecular timing data could be fit at all pressures with a model that incorporated regeneration of both the rotationally excited and the thermal levels in the afterglow. Interestingly, one of the arguments that Callear and Hedges advanced to refute a regeneration scheme was their difficulty in reconciling the exact second-order decay of the overall metastable population with regeneration. This work has shown directly that the two pictures can simultaneously occur without conflict.

The rate constant for metastable-metastable collision, k_{MM}, was determined from these experiments to be $(5\pm1)\times10^{-10}$ cm^3/s near 4.2 K. This reaction rate was found to be independent of pressure, consistent with the results of all previous researchers. The rate is very close to the values determined in the liquid-helium experiments, but considerably lower than that obtained by Pitchford, Taylor, and Collins [55] or Deloche *et al.* [56] in low-pressure room-temperature experiments. The value is higher than that determined in a high-pressure room-temperature discharge by Myers and Cunningham [57], whose measurement was successfully used in the analysis of the data taken by Emmert *et al.* [35] as well. Fugol, Grigorashchenko, and Myshkis [52] measured the rate of the ionizing interaction between two ^3S metastable atoms at temperatures as low as 10 K and found only a small change in the rate constant with temperature, so we might expect that the value of k_{MM} determined in this work to be comparable to the room-temperature values. Much of the discrepancy can surely be attributed to the lack of information about the matrix elements needed to convert the absorption data to a number density in the previous experiments. However, the omission of the possibility of regeneration could affect the result of Myers and Cunningham (both Pitchford, Taylor, and Collins and Deloche *et al.* had included regeneration terms in their models). Regeneration was crucial both in the extraction of the rate constant from the data in this experiment and for a consistent explanation of the timing behavior of various molecular populations.

The values obtained for the regeneration ratios f_n were observed to be roughly in proportion to the intensity of their associated spectral lines. When the f_n values are summed for a single pressure, using the proportionality to interpolate the ratios for the spectral lines not measured, and ignoring the inconsistent results of the ^3S atom regeneration, the result is always close to 0.50, the maximum allowed value; clearly, this process is extremely efficient at 4.2 K. This observation is consistent with the findings of other researchers in the field; Pitchford, Taylor, and Collins; Deloche *et al.*; and Johnson and Gerardo [50] found the efficiency of conversion of atomic and molecular ions formed in the afterglow back into metastable species to range from 50% to 100%, depending on the species and experimental conditions, with most measurements closer to 100%.

The regeneration ratios obtained in these experiments are related to the rate of recombination of electrons with ions in the afterglow. This rate is known to be dependent on the temperature of the electrons in the plasma [30,31] and may not necessarily be constant during the afterglow [13]. The ratios, then, represent an average rate of regeneration (and hence of recombination) over the span of a timing curve.

B. Experiments on the ^3S metastable atom

Timing data for the ^3S metastable atom could not be conclusively analyzed. The density of this species fell rapidly when the beam was terminated, but exhibited a definite long-term component, especially in the high-pressure data. The data were well modeled at every pressure by assuming a first-order decay process, and regeneration through metastable-metastable collisions, but the parameters so obtained could not be interpreted. The most closely related measurement was made in the electron-irradiated liquid-helium experiments [9]. In that work, as in ours, this species decayed faster than the other metastables, and a purely exponential decay with a time constant of 15 μs was reported. The authors found that the decay of the vibrationally excited species was roughly exponential as well, but with an evident delay in the beginning of the timing curve that could be attributed either to regeneration or to the response time of their detection system. They speculated that the regeneration could be due to interactions of the ^3S atom with the neighboring helium, but could not be conclusive on this point. Our timing results show no delay in the decay of the vibrationally excited species and no evidence of regeneration from the metastable atom.

C. The formation of metastable He_2 in a 4.2-K plasma

Metastable molecules have been observed to form initially in rotationally excited states by several different

researchers: first by Callear and Hedges [4] and by Stahlberg *et al.* [37] and Emmert *et al.* [35]. At 300 K, each of these groups have reported a rapid relaxation of the rotational levels into a thermal distribution through collisions with the background helium gas. This work has shown that the rotationally excited population does not appear to relax at all through collisions with the background gas at 4.2 K, a reasonable conclusion to reach from qualitative extrapolation of Callear and Hedges's experiments in a 77-K helium plasma. Interestingly, the initial rotational distribution of the species is nearly the same in both the liquid- and the gas-phase measurements at all temperatures, peaking at the $N=17$ rotational level [71]. Vibrationally excited molecules, on the other hand, have only been observed in the 4.2-K gas spectra, and in the electron-irradiated liquid spectra. In both cases, the observed transition has been the $b\ ^3\Pi_g \leftarrow a\ ^3\Sigma_u^+$. Most other experiments have monitored the visible $e\ ^3\Pi_g \leftarrow a\ ^3\Sigma_u^+$ absorption band, which leads to the speculation that perhaps the vibrationally excited levels can be formed at higher temperatures, but cannot be detected with visible absorption because of the nature of the upper vibrational levels of the $e\ ^3\Pi_g$ state.

The observation of rotationally and vibrationally excited populations existing in the $a\ ^3\Sigma_u^+$ state at 4.2 K leads naturally to questions regarding the formation processes for the various observed levels. We have convincing evidence to suggest that the three population groups are formed in different ways. Although the vibrationally excited and rotationally excited levels are both shown to grow in quickly and almost linearly immediately after the proton beam strikes the sample, in the afterglow the rotationally excited species have been shown to undergo regeneration, while the vibrationally excited species do not. This difference indicates separate formation mechanisms for these two species. The thermal levels show a stronger qualitative difference; they grow in nonlinearly from a zero slope at the time the proton beam enters the cell, and experience such strong regeneration in the afterglow that a noticeable bulge can be seen in the timing curves for this species. Such behavior leads to the conclusion that regeneration from metastable-molecule collision products is the only mechanism that feeds the thermal levels in the 4.2-K plasma, in contrast to plasmas at warmer temperatures where the population of thermal levels can be more readily explained by rotational relaxation of the rotationally excited species.

The last point raises a fundamental question about the dynamics of the helium afterglow at 4.2 K: How can thermal levels be formed from collisions involving rotationally and vibrationally excited species? How can such a reaction dispose of the excess angular momentum or vibrational energy to leave a rovibrationally cold product? To address these questions, we must first consider the nature of the He_2 Rydberg system itself, and make a few reasonable assumptions about the nature of the ionizing collision between metastables.

In the He_2 Rydberg molecule, the interaction between the core and the Rydberg electron is not very strong, since the potential curve of the ionic core is not significantly different from that of the Rydberg states. When such a system is ionized, the Rydberg electron will be ejected, but the internal state of the nuclear core may not change significantly. Thus, in a collision between two rovibrationally excited molecules, one should collapse into two ground-state atoms, and the other should produce an ion with essentially the same rovibrational parameters as the parent neutral molecule.

The Rydberg electron must also be responsible for shielding the ionic core from perturbation through collision with the background helium gas. Callear and Hedges proposed this idea to explain the dramatic decrease in the rotational relaxation rate of the $a\ ^3\Sigma_u^+$ state between 300 and 77 K. The principle is similar to the repulsive interaction between the outer electron of the ^3S atom and a ground-state helium atom that explains the repulsive hump in the potential of the $a\ ^3\Sigma_u^+$ state [72]. Such an assumption can certainly explain the absence of rotational relaxation of the neutral molecules observed in these experiments.

When an ionizing reaction occurs, the rovibrational state of the ion core is no longer "protected" from change by the Rydberg electron. Frequent collisions with the background helium gas can now effect changes in the rovibrational state of the molecule, thermalizing the core. Neutralization of these cooled ion cores could lead to the thermal population observed in these experiments.

From the literature, we know that the dominant ion at 4.2 K should be He_3^+, formed either from a three-body reaction between a He_2^+ ion and two helium atoms, or a four-body reaction between a He^+ ion and three helium atoms, and its recombination should be responsible for at least one of the excited species. As we mentioned in Sec. II, this suggestion has been put forward by several different authors in the past, and Gerardo and Gusinow [30] suspected that the recombination products were an excited He_2 molecule and a helium atom. The neutralization of this species is attractive as a progenitor for the rotationally excited metastables for two principal reasons. First, no unwieldy explanations need be offered for the generation of the rotational angular momentum, since the dissociative neutralization of He_3^+ can conceivably leave a rotating molecule and eject a helium atom. In contrast, neutralization of a He_2^+ ion to generate these species implies a rotationally excited precursor, with no explanation for how that excitation was imparted to the ion. Secondly, the fact that the rotationally excited species are vibrationally cool would be rationalized.

The He_3^+ ion must be able to reform in the afterglow for this mechanism to be valid for the production of rotationally excited metastables. If the ionizing collision leaves the core of one of the participant molecules essentially undisturbed, then this core will be either rotationally or vibrationally excited, or thermalized. Reformation of the triatomic ion from the first two species does not seem likely; one can see particularly the difficulties in attaching a third atom to a rapidly rotating core. However, three-body collisions involving a thermalized core should generate the required ion, and regenerate rotationally excited metastables in the afterglow. Such a process is also consistent with the observation that the regeneration ratios are in rough proportion to the intensity of

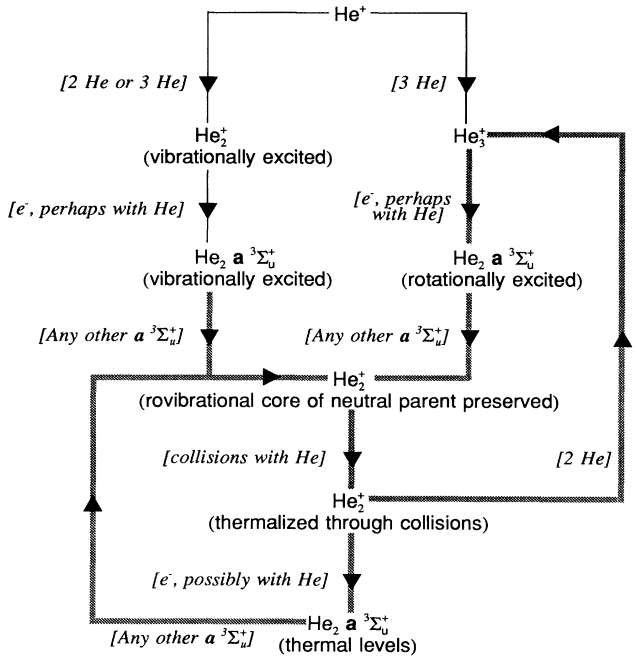

FIG. 11. A diagram of the reaction pathways active in the 4.2-K helium plasma studied in this experiment. Pathways drawn in thin lines are active only while the proton beam stimulates the sample. Those drawn in thick lines are active during the afterglow as well.

their associated absorption lines.

Since the He_2^+ ion has been commonly thought to form in highly vibrationally excited states through collision of a He^+ ion and two ground-state atoms, this species could form a vibrationally excited neutral. The reaction (2.1) between a ^3S atom and two ground-state helium atoms was not observed to form any metastable-molecule species in these experiments, consistent with the work of Köymen *et al.* [16], in which reaction (2.1) could not be detected at temperatures below 65 K [17]. One might question why vibrationally excited helium does not reform in the afterglow, like the rotationally excited and thermal levels. If the parent species is a He_2^+ ion formed from reactive collisions of a He^+ ion and two helium atoms, then vibrationally excited species will not reform if He^+ ions are not products of the collisions between metastable molecules; such a situation is, in fact, quite likely. Deloche *et al.* [56] found that the fraction of He^+ ion products formed from these collisions lay between 0% and 30%, and Emmert *et al.* [35] assumed a value of 15%. These determinations were made at 300 K and room temperature; if at cryogenic temperatures the fraction decreased further, then this condition would be met.

The ideas presented in this subsection have been summarized as a diagram of the reaction pathways in Fig. 11. The primary ions and neutral species involved in the reaction cycle are connected with paths, and the species necessary for the associated reaction are listed beside each path. The processes active only while the proton beam is on the sample are marked with thin lines, while those active during the afterglow as well are drawn with thick lines. The diagram demonstrates the rich and interesting behavior of the helium plasma that was studied in these experiments.

One of the larger uncertainties in a work such as this is the effect of temperature variations across the sample cell when the proton beam is on. These arise because of the low thermal conductivity of a gas near 4.2 K. In fact, the magnitude of this effect was not realized until the study was completed and in retrospect the use of a single proton-beam energy, a single beam current, and for that matter a single sample cell would have been desirable. Though we believe such thermal effects do not invalidate any of the results presented here, it is possible that such effects contribute to the systematic errors noticeable in some of the Tables.

In this work, we have formulated a picture of the afterglow that is consistent with our experimental results, and with much of the work in the existing spectroscopic and plasma literature. We have also made a determination of k_{MM}, the rate of ionizing collision between metastable-molecule species. Further work on the ion processes, particularly on the products produced by He_3^+ neutralization, would be helpful in clarifying their role in a helium afterglow.

ACKNOWLEDGMENTS

The authors gratefully acknowledge many useful and informative discussions with Dr. B. G. Nickel. Comments and suggestions from Dr. F. B. Dunning, who read this material in thesis form, are also kindly acknowledged. The assistance of Dr. J. J. Miller, J. A. Forrest, and J. P. Voroney was also appreciated, as was the technical support of the McMaster Tandem Accelerator staff, and W. Teesdale at Guelph. One of us (D.W.T.) also wishes to acknowledge the cooperation of the Department of Physics, and University Computing Services, at the University of Newcastle, NSW, Australia, in the preparation of this manuscript. This research is supported by the Natural Sciences and Engineering Research Council of Canada (NSERC).

[1] R. L. Brooks and J. L. Hunt, J. Chem. Phys. **88**, 7267 (1988).
[2] R. L. Brooks, J. L. Hunt, and D. W. Tokaryk, J. Chem. Phys. **91**, 7408 (1989).
[3] A. B. Callear and R. E. M. Hedges, Nature **215**, 1267 (1967).
[4] A. B. Callear and R. E. M. Hedges, Trans. Faraday Soc. **66**, 2921 (1970).
[5] W. S. Dennis, E. Durbin, Jr., W. A. Fitzsimmons, O. Heybey, and G. K. Walters, Phys. Rev. Lett. **23**, 1083 (1969).
[6] J. C. Hill, O. Heybey, and G. K. Walters, Phys. Rev. Lett. **26**, 1213 (1971); erratum **26**, 1519 (E) (1971).

[7] C. M. Surko and F. Reif, Phys. Rev. **175**, 229 (1968).
[8] J. W. Keto, M. Stockton, and W. A. Fitzsimmons, Phys. Rev. Lett. **28**, 792 (1972).
[9] J. W. Keto, F. J. Soley, M. Stockton, and W. A. Fitzsimmons, Phys. Rev. A **10**, 872 (1974).
[10] J. W. Keto, F. J. Soley, M. Stockton, and W. A. Fitzsimmons, Phys. Rev. A **10**, 887 (1974).
[11] A. V. Phelps, Phys. Rev. **99**, 1307 (1955).
[12] J. E. Lawler, J. W. Parker, L. W. Anderson, and W. A. Fitzsimmons, Phys. Lett. A **69**, 408 (1979).
[13] J. Stevefelt, J. M. Pouvesle, and A. Bouchoule, J. Chem. Phys. **76**, 4006 (1982).
[14] A. V. Phelps and J. P. Molnar, Phys. Rev. **89**, 1202 (1953).
[15] Kenneth L. Ludlum, Lewis P. Larson, and James M. Caffrey, Jr., J. Chem. Phys. **46**, 127 (1967).
[16] A. Köymen, F.-C. Tang, X. Zhao, F. B. Dunning, and G. K. Walters, Chem. Phys. Lett. **168**, 405 (1990).
[17] F. B. Dunning and X. Zhao (private communication).
[18] C. P. de Vries and H. J. Oskam, Phys. Rev. A **22**, 1429 (1980).
[19] John A. Hornbeck and J. P. Molnar, Phys. Rev. **84**, 621 (1951).
[20] Robert S. Mulliken, Phys. Rev. A **136**, 962 (1964).
[21] M. D'Angelo, Phys. Rev. **121**, 505 (1961).
[22] For a recent example of this work, see Y. S. Cao and R. Johnsen, J. Chem. Phys. **94**, 5443 (1991).
[23] P. L. Patterson, J. Chem. Phys. **48**, 3625 (1968).
[24] E. E. Ferguson, D. B. Dunkin, F. C. Fehsenfeld, and A. L. Schmeltekopf, Bull. Am. Phys. Soc., Sec. II **13**, 212 (1968).
[25] R. A. Gerber and M. A. Gusinow, Phys. Rev. A **4**, 2027 (1971).
[26] K. Balasubramanian, M. Z. Liao, and S. H. Lin, Chem. Phys. Lett. **142**, 349 (1987).
[27] Marzio Rosi and Charles W. Bauschlicher, Jr., Chem. Phys. Lett. **159**, 479 (1989).
[28] Oum Keltoum Kabbaj, Marie-Bernadette Lepetit, and Jean-Paul Martin, Chem. Phys. Lett. **172**, 483 (1990).
[29] M. A. Gusinow, R. A. Gerber, and J. B. Gerardo, Phys. Rev. Lett. **25**, 1248 (1970).
[30] J. B. Gerardo and M. A. Gusinow, Phys. Rev. A **3**, 255 (1971).
[31] J.-F. Delpech and J.-C. Gauthier, Phys. Rev. A **6**, 1932 (1972).
[32] D. R. Bates, J. Phys. B **12**, L35 (1979).
[33] D. R. Bates, J. Phys. B **17**, 2363 (1984).
[34] C. B. Collins and W. B. Hurt, Phys. Rev. **179**, 203 (1969).
[35] F. Emmert, H. H. Angermann, R. Dux, and H. Langhoff, J. Phys. D **21**, 667 (1988).
[36] V. I. Derzhiev, V. S. Skakun, V. F. Tarasenko, S. I. Yakovlenko, and A. M. Yancharina, Opt. Spektrosk. **64**, 506 (1988) [Opt. Spectrosc. (USSR) **64**, 303 (1988)].
[37] Birger Stahlberg, Valery M. Baev, Gerhard Gaida, Holger Schröder, and Peter E. Toschek, J. Chem. Soc., Faraday Trans. 2 **81**, 207 (1985).
[38] V. A. Ivanov and Yu. E. Skoblo, Opt. Spektrosk. **65**, 750 (1988) [Opt. Spectrosc. (USSR) **65**, 445 (1988)].
[39] C. B. Collins and B. W. Johnson, J. Chem. Phys. **56**, 1563 (1972).
[40] C. B. Collins and B. W. Johnson, J. Chem. Phys. **64**, 2605 (1976).
[41] J.-C. Gauthier, J.-P.Geindre, J.-P. Moy, and J.-F. Delpech, Phys. Rev. A **13**, 1781 (1976).
[42] J. C. Polanyi and K. B. Woodhall, J. Chem. Phys. **56**, 1563 (1972).
[43] Satoshi Takao, Masuhiro Kogoma, Takefumi Oka, Masashi Imamura, and Shigeyoshi Arai, J. Chem. Phys. **73**, 148 (1980).
[44] K. W. Meissner and W. Graffunder, Ann. Phys. (Leipzig) **84**, 1009 (1927).
[45] Edgar Ebbinghaus, Ann. Phys. (Leipzig) **7**, 267 (1930).
[46] Manfred A. Biondi, Phys. Rev. **82**, 453 (1951).
[47] Manfred A. Biondi, Phys. Rev. **88**, 660 (1952).
[48] R. W. Huggins and J. H. Cahn, J. Appl. Phys. **38**, 180 (1967).
[49] Kenneth H. Ludlum, James. M. Caffrey, Jr., and Lewis P. Larson, J. Opt. Soc. Am. **58**, 269 (1968).
[50] A. Wayne Johnson and J. B. Gerardo, Phys. Rev. A **7**, 925 (1973).
[51] Gary Myers and A. J. Cunningham, J. Chem. Phys. **67**, 247 (1977).
[52] I. Ya. Fugol, O. N. Grigorashchenko, and D. A. Myshkis, Zh. Eksp. Teor. Fiz. **60**, 423 (1971) [Sov. Phys. JETP **33**, 227 (1971)].
[53] W. A. Fitzsimmons, N. F. Lane, and G. K. Walters, Phys. Rev. **174**, 193 (1968).
[54] Michèle Jardino, Francis Lambert, and Robert Deloche, C. R. Acad. Sci. (Paris) **278B**, 1087 (1974).
[55] L. C. Pitchford, K. N. Taylor, and C. B. Collins, J. Phys. B **8**, 142 (1975).
[56] R. Deloche, P. Monchicourt, M. Cheret, and F. Lambert, Phys. Rev. A **13**, 1140 (1976).
[57] G. Myers and A. J. Cunningham, J. Chem. Phys. **67**, 1942 (1977).
[58] David R. Yarkony, J. Chem. Phys. **90**, 7164 (1990).
[59] *Physics Vade Mecum,* edited by Herbert L. Anderson (American Institute of Physics, NY, 1981).
[60] W. L. Wiese, *Atomic Transition Probabilities,* Natl. Bur. Stand. (U.S.) Circ. No. 4 (U.S. GPO, Washington, DC, 1966), Vol. I.
[61] Ellis E. Whiting, Aert Schadee, Jeremy B. Tatum, Jon T. Hougen, and Ralph W. Nicholls, J. Mol. Spectrosc. **80**, 249 (1980).
[62] Ellis E. Whiting and Ralph W. Nicholls, Astrophys. J. Suppl., No. 235, **27**, 1 (1974).
[63] Robert J. LeRoy, University of Waterloo Chemical Physics Research Report No. CP-330, 1991 (unpublished).
[64] Jon T. Hougen, Nat. Bur. Stand. Monogr. (U.S.) **115**, (1970).
[65] I. Kovacs, *Rotational Structure in the Spectra of Diatomic Molecules* (Adam Hilger Ltd., London, 1969).
[66] Aert Schadee, J. Quant. Spectrosc. Radiat. Transfer **19**, 451 (1978).
[67] S. A. Rogers, C. R. Brazier, P. F. Bernath, and J. W. Brault, Mol. Phys. **63**, 901 (1988).
[68] A. P. Thorne, *Spectrophysics* (Chapman and Hall Ltd., London, 1974).
[69] Philip R. Bevington, *Data Reduction and Error Analysis for the Physical Sciences* (McGraw-Hill, New York, 1969).
[70] M. A. Gusinow and R. A. Gerber, Phys. Rev. A **2**, 1973 (1970).
[71] Keto *et al.* [9] indicate that the $N=13$ level is the most heavily populated rotational level in their liquid spectrum in the text of their paper, but the P-branch distribution is identical to the gas spectra, and the low resolution of the other branches makes such estimates crude.
[72] Steven L. Guberman and William A. Goddard III, Phys. Rev. A **12**, 1203 (1975).